Clay Minerals (2024), 1–7
doi:10.1180/clm.2023.36

CAMBRIDGE UNIVERSITY PRESS

Article

Synthesis and characterization of nano-silica from locally available laterite clay

Safeena Khattak[1], Saeed Gul[2], Sabiha Sultana[3,4] and Noor-ul-Amin[1]

[1]Department of Chemistry, Abdul Wali Khan University, Mardan, Pakistan; [2]Department of Chemical Engineering, University of Engineering and Technology, Peshawar, Pakistan; [3]Department of Chemistry, Islamia College University, Peshawar, Pakistan and [4]University of Exeter, Penryn Campus, Penryn, UK

Abstract

The synthesis of nano-silica is gaining the attention of researchers due to its numerous applications in various fields such as medicine, the food industry, catalysis, agriculture and construction, amongst others, because of its unique physicochemical features. However, achieving its facile synthesis and finding inexpensive source material that is locally available requires further exploration for its large-scale production. This paper reports the synthesis and characterization of nano-silica from locally available laterite clay using the sol-gel method. The product was analysed using X-ray florescence, X-ray diffraction, Fourier-transform infrared spectroscopy, scanning electron microscopy and transmission electron microscopy. It was observed that the product was spherical, agglomerated and amorphous in nature. The obtained nano-silica was found to have 97% and 95% purity for sodium hydroxide and potassium hydroxide, respectively. The synthesized nano-silica is expected to play pivotal role as a pozzolanic activator in the construction industry.

Keywords: Laterite clay; nano-silica; potassium hydroxide; sodium hydroxide; sodium silicate

(Received 5 July 2023; revised 15 December 2023; accepted 16 December 2023; Associate Editor: Chunhui Zhou)

Nanomaterials play a vital role in binding and in the construction industry. Different nano-materials, such as nano-silica (She *et al.*, 2018; Luo *et al.*, 2019), nano-alumina (Heikal *et al.*, 2015), nano-iron (Heikal, 2016), nano-$CaCO_3$ (Meng *et al.*, 2017), nano-calcium silicate hydrate seeds (Kanchanason & Plank, 2017), and carbon nanotubes and fibres (Sikora *et al.*, 2019), amongst other, have been studied to improve the mechanical parameters and durability of cement composites (Singh *et al.*, 2017). Nano-silica has become more attractive to material chemistry and material engineering researchers because of its exceptional properties such as its small particle size, great surface area and surface activity (Tang *et al.*, 2014). Based upon the unique nature of silica, it has various properties; for example, it is acidic and hydrophilic due to the presence of surface silanol groups (Jafarzadeh *et al.*, 2009) and it exhibits agglomeration due to Van der Waals forces and hydrogen bonds between surface hydroxyl groups (Sun *et al.*, 2013), thus reducing its compatibility with organic polymers.

The parameters of the obtained silica, irrespective of the starting material, depends on the method of its manufacture, such as the precipitation method (Norsuraya *et al.*, 2016), thermal synthesis (Yuvakkumar *et al.*, 2014) and the sol-gel method (Gu *et al.*, 2015), amongst others. It is one of the most promising environmentally friendly and economically valuable fillers, and it can also be prepared from renewable sources such as ashes from biomasses, including bagasse ash of sugarcane and rice husks (Tang *et al.*, 2016). However, achieving a consistent supply of raw materials for its large-scale production is challenging. Therefore, there is a need to explore such raw materials that are locally available in abundance and can be supplied consistently for the large-scale production of nano-silica.

The main aim of the present investigation was to develop a facile procedure for the preparation of nano-silica from cheap and locally available laterite clay, as no such work has been documented in the published literature. In the present study, we prepared nano-silica from laterite clay in the nanometre range. The alumina content in the precursor was reduced *via* a series of thermal and acid treatments. Various parameters, such as the thermal activation temperature of the laterite clay, were optimized, and alkali solutions were used to determine the greatest percentage yield of nano-silica samples with purities of 97% and 95% for sodium hydroxide and potassium hydroxide.

Materials

Laterite clay samples were collected from the surroundings of Askari Cement Ltd, Wah District, Pakistan. Methanol (CH_3OH; 99%) was purchased from RDH, sodium hydroxide (NaOH; 99%) and potassium hydroxide (KOH; 98%) were purchased from Sigma-Aldrich and hydrochloric acid (HCl; 37%) was purchased from Merck. Deionized water was prepared at our own laboratory.

Methods

Extraction of nano-silica

Laterite clay was thermally activated at various temperatures (650°C, 700°C and 750°C) for a period of 1 h using a programmable tube

Corresponding author: Noor-ul-Amin; Email: noorulamin@awkum.edu.pk
Cite this article: Khattak S, Gul S, Sultana S, Noor-ul-Amin. Synthesis and characterization of nano-silica from locally available laterite clay. *Clay Minerals*. https://doi.org/10.1180/clm.2023.36

furnace (BEQ-China) with a temperature increment rate of 5°C min^{-1}.

Laterite clay was washed using HCl to remove other metals prior to the extraction of nano-silica. A 10 g laterite clay sample was dispersed in 100 mL of 2 M HCl and heated at a temperature of 120°C for a period of 2 h under constant stirring using a hotplate and then filtered off. The residue was washed with deionized water until the pH became 7 and then heated in oven at 120°C until complete drying was achieved.

The acid-washed samples of the laterite clay were treated with 3 M alkali solution. At this stage, NaOH and KOH were compared for their extraction efficiency; therefore, two set of solutions were prepared, one treated with 3 M NaOH and the other with 3 M KOH. The alkali-added solutions were then heated at a constant temperature of 120°C for 3 h a using a hotplate. The mixture was cooled to room temperature and then filtered using filter paper (Whatman-41). The filtrates containing sodium silicate and potassium silicate solutions were treated with 3:1 HCL and methanol, which was added dropwise until the formation of precipitates, and the pH of the solution was adjusted to 5. The reagent mixture was then filtered using filter paper (Whatman-42) and the obtained nano-silica was washed repeatedly to remove impurities. A graphical representation this process is given in Fig. 1.

Characterization

The purity of the nano-silica obtained from laterite clay was determined using the hydrofluoric acid (HF) test. For this purpose, 1 g of the obtained nano-silica was mixed with 0.5 mL of hydrofluoric acid in a platinum crucible and heated in a furnace at 1000°C until a constant weight was obtained. The residue was weighed after cooling in a desiccator. Purity was calculated using Equation 1.

$$\text{Purity} = \frac{\text{Loss in mass of silica}}{\text{Mass of silica taken in the crucible}} \times 100 \quad (1)$$

Elemental analysis of the as-received laterite clay and nano-silica samples was carried out using an X-ray fluorescence (XRF) spectrophotometer (Philips PW 2582/00). Nano-silica was characterized using Fourier-transform infrared (FTIR) spectroscopy (Shimadzu IR Prestige-21 spectrometer), X-ray diffraction (XRD; JEOL JDX-3532), scanning electron microscopy (SEM; JEOL JSM-5910) and transmission electron microscopy (TEM; JEOL JEM-2100).

The XRF spectrophotometer was utilized to study various compounds such as iron oxide, sodium oxide, alumina and others that were present in the as-received and acid-washed samples of laterite, as well as for the two samples of nano-silica that were prepared.

For the FTIR studies, a pure pellet of KBr was taken as a blank whilst thin pellets with a 5% solid solution of the sample with KBr were prepared. The region of the spectra selected was between 4000 and 400 cm^{-1}.

XRD of nano-silica was performed for the phase analysis, for which each sample was put in a glass holding device before being moved to the X-ray tube. Spectra were taken with a scanning range of 10–50°, a voltage of 35 kV and a current of 20 mA.

Morphological examination and size measurement of nano-silica was performed using SEM. For this purpose, silica was dispersed in ethanol and then dropped onto a glass slide followed by carbon coating. For the average particle size and standard deviation calculations, ~100 measurements were performed using SEM images of each sample.

For TEM analysis, a focused electron beam was passed through a very thin layer of the sample. The information obtained using TEM was identical to that from a transmission optical microscope, but the magnification and resolution were greater.

Results and discussion

XRF analysis of the laterite clay

The elemental composition of the laterite clay before and after the acid leaching as determined using XRF is given in Table 1. Table 1

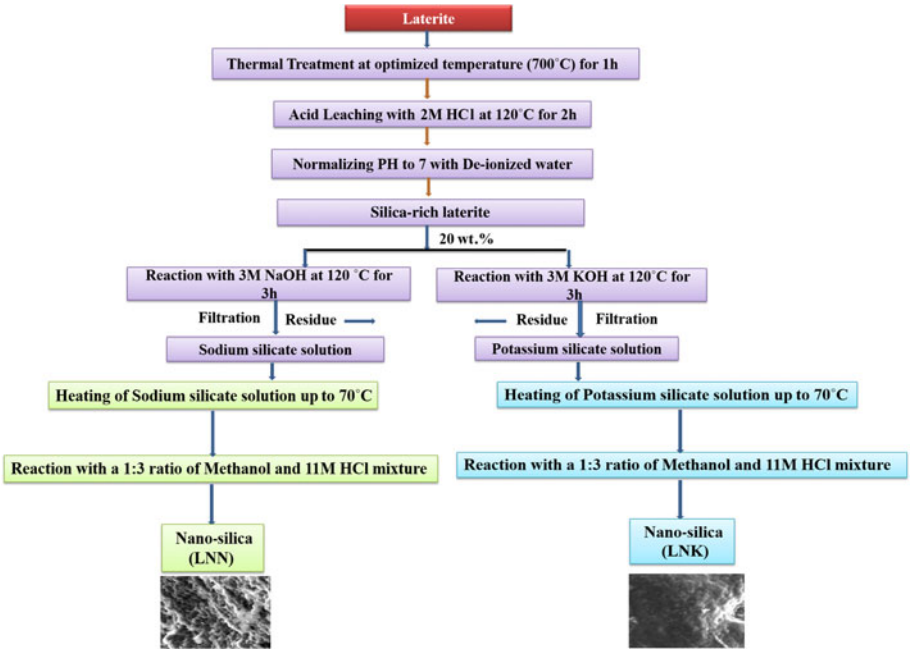

Figure 1. Flow chart representing the process for producing silica nanoparticles from laterite clay. LNK = nano-silica extracted using potassium hydroxide; LNN = nano-silica extracted using sodium hydroxide.

https://doi.org/10.1180/clm.2023.36 Published online by Cambridge University Press

Table 1. Composition of the laterite clay and extracted nano-silica analyzed using XRF.

Sample ID	Composition (wt.%)							
	SiO_2	Al_2O_3	Fe_2O_3	CaO	MgO	K_2O	Na_2O	SO_3
As-received laterite	17.47	6.28	34.41	28.88	0.880	0.580	1.08	0.07
Acid-leached laterite	51.03	2.03	6.830	11.04	1.920	1.020	2.03	1.07
Extracted nano-silica using sodium hydroxide	97.00	0.27	0.015	0.155	0.231	0.021	1.10	–
Extracted nano-silica using potassium hydroxide	95.00	0.25	0.015	0.255	0.231	1.021	1.50	–

shows that the as-received laterite contains silicon and aluminium as the major elements, whose concentrations in oxide form are 17.47% and 6.28% before acid leaching and 51.03% and 2.03% after acid leaching, respectively. Table 1 also indicates that a considerable decrease in the amount of alumina and an increase in the silica content occurred after acid treatment.

To make the raw clay reactive and to increase the percentage of silica, the laterite clay was thermally treated at various temperatures (650°C, 700°C and 750°C), and the elemental composition of nano-silica obtained from each treatment is shown in Fig. 2. From Fig. 2, it is clear that the sample calcined at 700°C become more reactive and gave the greatest nano-silica yield. It can be concluded that increasing the calcination temperature up to 700°C could increase the reactivity of laterite clay. The unfavourable production of nano-silica at temperatures >700°C might be due to the fact that at higher temperatures the laterite clay again becomes crystalline and less reactive. This reveals that for maximum extraction of nano-silica the laterite clay should not be thermally activated at >700°C, which is the optimum temperature for calcination.

HF analysis of the laterite clay

The purity of the prepared nano-silica was studied using the HF test, and the results are given in Table 2. Table 2 demonstrates that

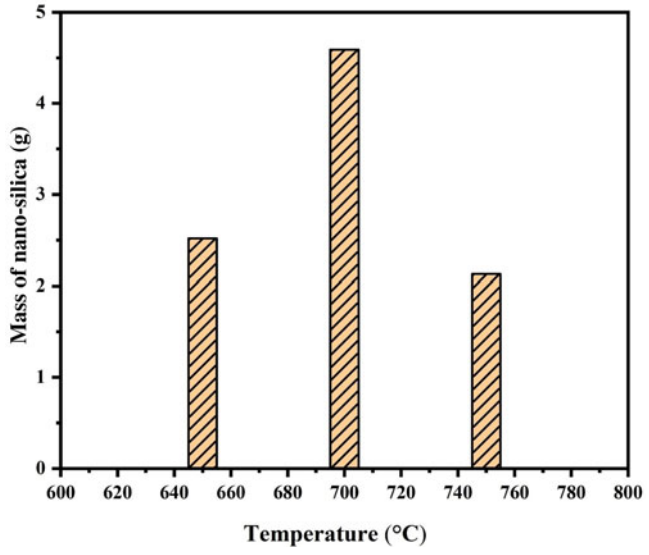

Figure 2. Nano-silica production as a function of calcination temperature.

Table 2. Purity of nano-silica based on the HF test.

	Nano-silica	
	Obtained using sodium hydroxide	Obtained using potassium hydroxide
Weight at beginning (g)	1.00	1.00
Weight loss (g)	0.97	0.95
Purity (%)	97	95

highly pure nano-silica obtained from laterite clay is 97% and 95% with respect to sodium hydroxide and potassium hydroxide, respectively. It is also observed that the purity of nano-silica resulting from sodium hydroxide is greater than that from potassium hydroxide under identical conditions. This finding is supported by previous studies showing that the purity of silica obtained from bagasse ash is 96% (Amin *et al.*, 2016) and that from corn cobs is 60.2% (Velmurugan *et al.*, 2015). The purity being <100% in this nano-silica could due to the presence of moisture and some impurities such as sodium, calcium and alumina, amongst others, as is clear from Table 2. The existence of moisture in this nano-silica could be due to imperfect drying after precipitation, whereas the presence of impurities might be due to insufficient acid being used for washing or incomplete washing of the laterite clay prior to the extraction of nano-silica.

FTIR analysis of nano-silica

The FTIR spectra of nano-silica obtained from thermally activated laterite clay at 700°C with sodium hydroxide and potassium hydroxide are shown in Figs 3 & 4, respectively. Figures 3 & 4 clarify that the primary silica absorption band occurs in the range 1300–800 cm^{-1}. The peak at ~3500–3300 cm^{-1} corresponds to the stretching and bending vibration of –OH absorbed from H_2O and silanol (Si–OH). Similarly, the peaks positioned in the range 1636–1631 cm^{-1} corresponds to the bending and stretching modes of OH. The bending mode of OH being greatly intensified in this spectrum region of 1636–1631 cm^{-1} supports the presence of Si–OH groups on the hydrophilic surfaces. The broad peak in the spectra, observed in the 1226–1063 cm^{-1} range, represents Si–O–Si asymmetric stretching vibrations. Similarly, the stretching vibration in the range of 955–950 cm^{-1} corresponds to the surface –OH group of silanol. The minor peaks at ~802–791 cm^{-1} correspond to the symmetrical stretching of Si–O–Si linkages in the $Si–O_4$ network, whereas the band at ~470–446 cm^{-1} confirms the presence of Si–O–Si linkages in siloxane bond bending vibrations. In addition to Si–O–Si and Si–OH, the mean intensity of the –OH stretching and bending peaks increase in nano-silica with respect to potassium hydroxide. These findings regarding peak positioning for the various functional groups are supported by the previous research (Ghorbani *et al.*, 2013; Wang *et al.*, 2010).

XRD analysis of nano-silica

The XRD traces of nano-silica produced from thermally activated laterite clay at 700°C with sodium hydroxide and potassium hydroxide are shown in Figs 5 & 6, respectively. The patterns correspond to the amorphous nature of nano-silica. Figures 5 & 6 show one broad hill-shaped diffraction peak ranging from 22° to 23°2θ, providing evidence in support of the amorphous nature of the nano-silica obtained using both sodium hydroxide and

https://doi.org/10.1180/clm.2023.36 Published online by Cambridge University Press

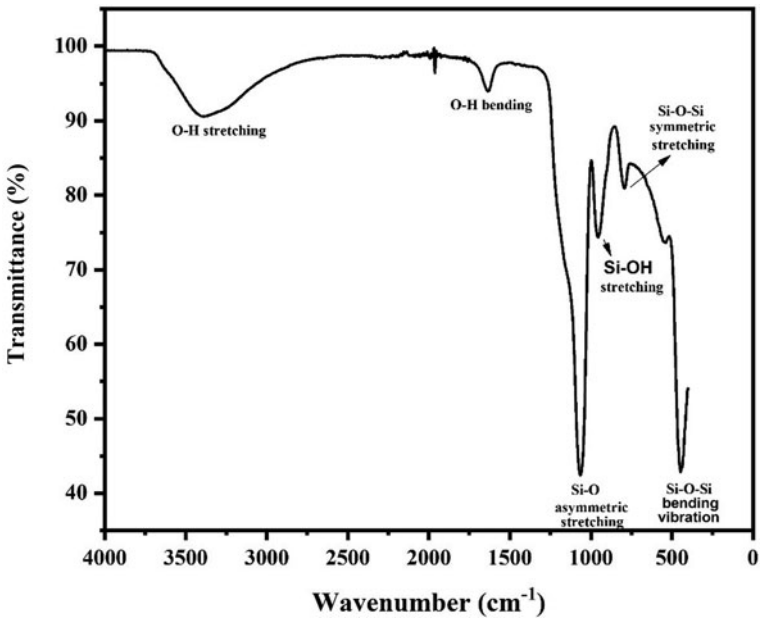

Figure 3. FTIR spectrum of nano-silica extracted from laterite clay using sodium hydroxide.

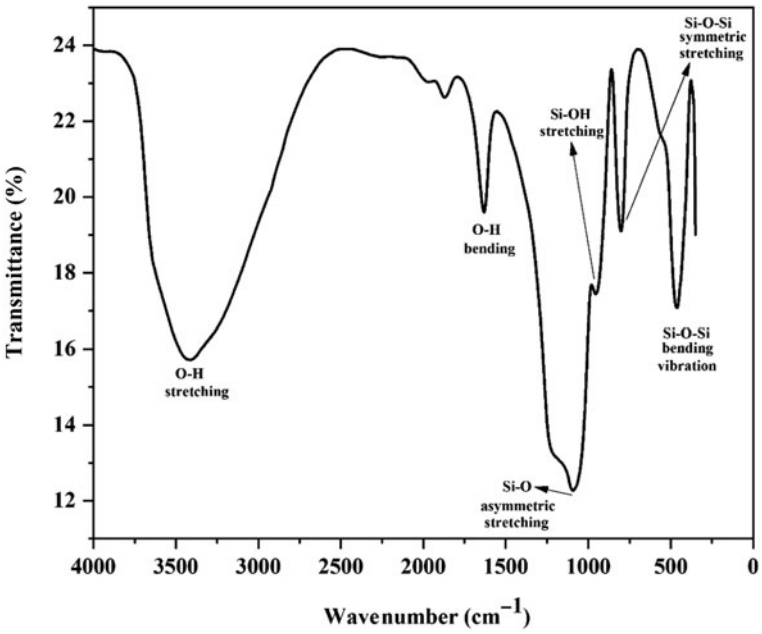

Figure 4. FTIR spectrum of nano-silica extracted from laterite clay using potassium hydroxide.

potassium hydroxide (Zhang *et al.*, 2021). An important observation from the XRD traces is that the broad peak (Fig. 5) shifts towards a lower °2θ value (Fig. 6) with increasing water content. The greater hydroxyl groups present in silica make it less viscid and leads to a wobbly packing structure, which reduces the density of the samples. As a result, the density of nano-silica obtained with potassium hydroxide underwent less of change as compared to that obtained with sodium hydroxide. This effect is also evident from the FTIR spectra (Figs 3 & 4), which show more intense hydroxyl group peaks for nano-silica obtained using potassium hydroxide than nano-silica obtained using sodium hydroxide. These findings are also supported by the previous literature (Wassie & Srivastava, 2017). Figure 6 shows that the peaks at 25°2θ and 38°2θ, as shown in Fig. 5 regarding sodium hydroxide, became greatly diminished, thus reducing inactive nano-silica, as has been reported in previous work of a similar nature (Paya *et al.*, 2001).

SEM analysis of nano-silica extracted from the laterite clay

Figure 7 shows SEM images of the surface morphology of extracted nano-silica powders under optimized conditions with sodium hydroxide and potassium hydroxide. It can be observed from Fig. 7 that homogeneous clusters of particles are seen that are dissimilar in size. Greatly magnified images reveal that the large clusters of particles are the agglomerations of a large number of smaller particles.

https://doi.org/10.1180/clm.2023.36 Published online by Cambridge University Press

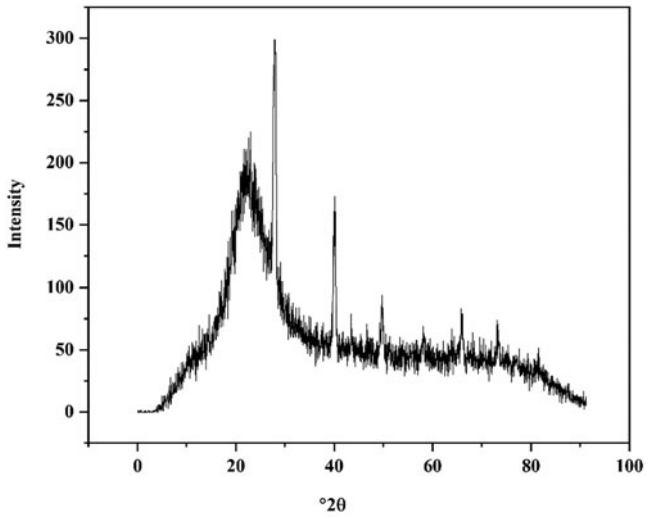

Figure 5. XRD trace of nano-silica extracted from laterite clay using sodium hydroxide.

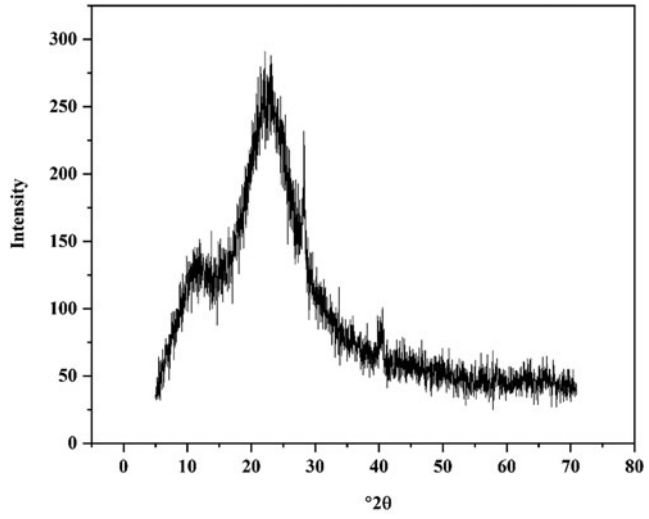

Figure 6. XRD trace of nano-silica extracted from laterite clay using potassium hydroxide.

TEM analysis of nano-silica extracted from the laterite clay

To determine the particle size of the resultant nano-silica, TEM at much higher magnification and resolving power than SEM was used, and the resultant images are shown in Figs 8 & 9 for sodium hydroxide and potassium hydroxide, respectively. Figures 8a & 9a show the TEM images, while Figs 8b & 9b show the TEM histograms that display the approximate grain size of the nano-silicas derived with sodium hydroxide and potassium hydroxide, respectively. To estimate more accurately estimate the size of the particles, *ImageJ* software was used to analyse the TEM images. From the software application on the TEM images, it was confirmed that the particle size of the nano-silica obtained using sodium hydroxide is smaller than that obtained using potassium hydroxide. The particle sizes using both of these alkalis are in nano range, being on average 41.0 and 52.6 nm with sodium and potassium hydroxide, respectively. Similar studies have been conducted using zinc oxide nanoparticles and the same behaviour of size reduction was observed when the alkali used was changed from sodium hydroxide to potassium hydroxide (Ghorbani *et al.*, 2013).

Conclusion

Nano-silica was effectively extracted from laterite clay in the particle size range of 41.0 and 52.6 nm on average using sodium hydroxide and potassium hydroxide, respectively. The optimum temperature for the calcination of laterite clay was found to be 700°C. The thermally activated clay after undergoing a sequence of acid and thermal processes was activated with sodium hydroxide and potassium hydroxide solution to prepare sodium silicate and potassium silicate solutions. Nano-silica particles were obtained by reacting the sodium silicate and potassium silicate solutions with hydrochloric acid along with the addition of ethanol. It was observed that the temperature of thermal treatment had a great impact on the production of nano-silica. Moreover, the selection of the alkali used had a great impact on the morphology, crystallinity and particle size of the extracted nano-silica. The particle size of nano-silica was smaller when obtained using sodium hydroxide in comparison to that obtained using potassium hydroxide, probably due to the absorption of more water as indicated by the intensified FTIR spectra peaks for –OH groups when obtained with potassium hydroxide. The nano-silica particles were spherical, dissimilar in

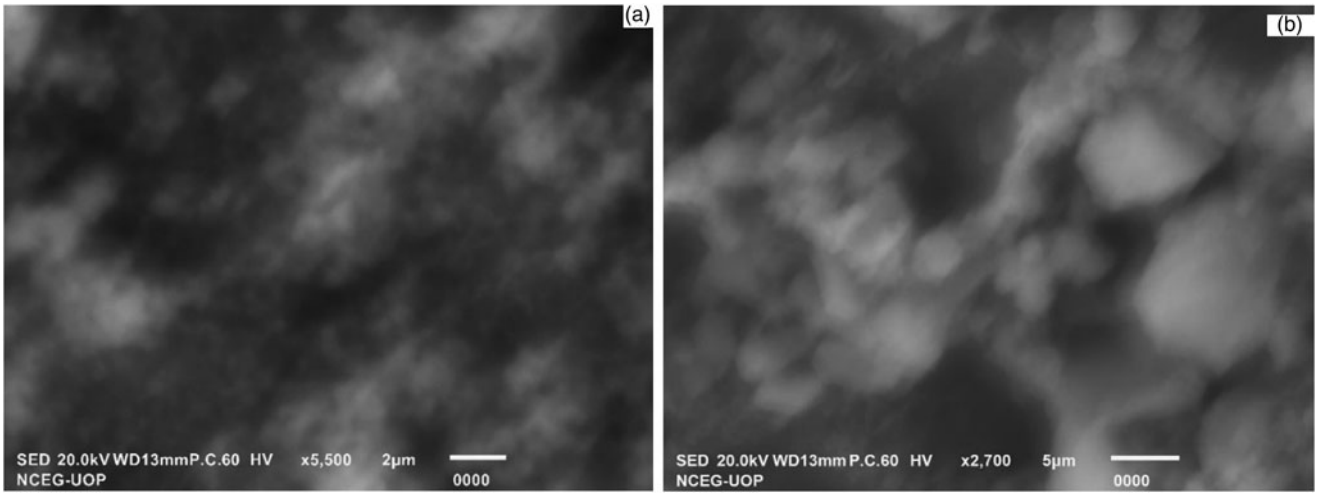

Figure 7. SEM images of nano-silica synthesized from laterite clay using (a) sodium hydroxide and (b) potassium hydroxide.

https://doi.org/10.1180/clm.2023.36 Published online by Cambridge University Press

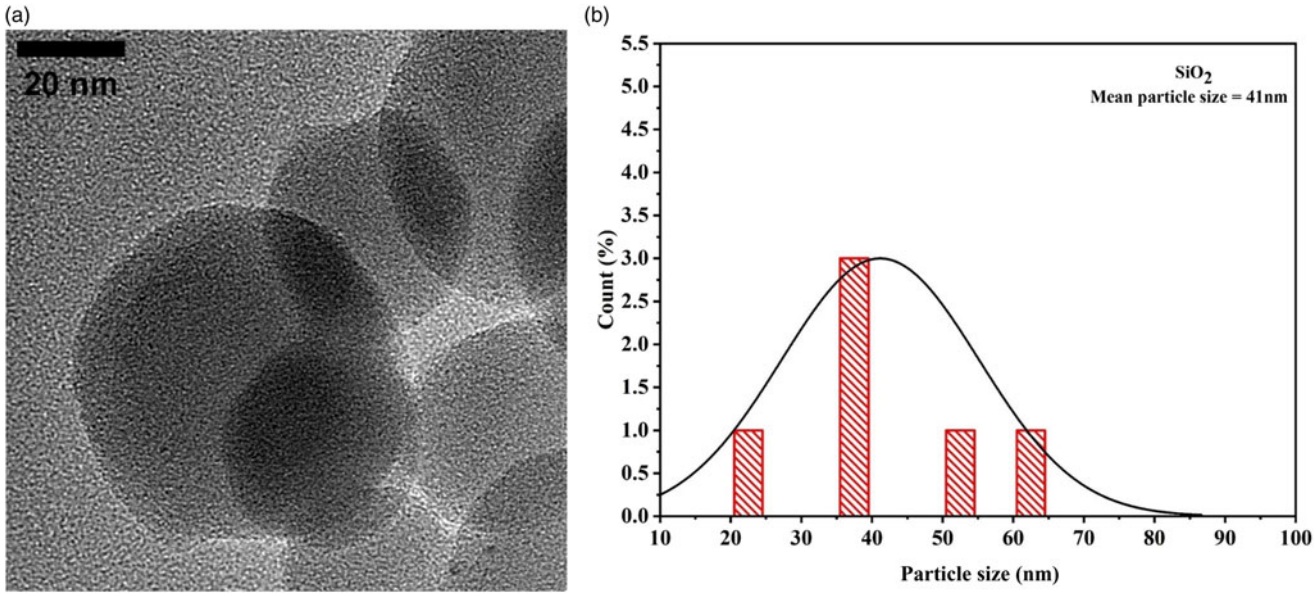

Figure 8. (a) TEM image of silica nanoparticles with sodium hydroxide. (b) Particle-size distribution histogram of silica nanoparticles with sodium hydroxide.

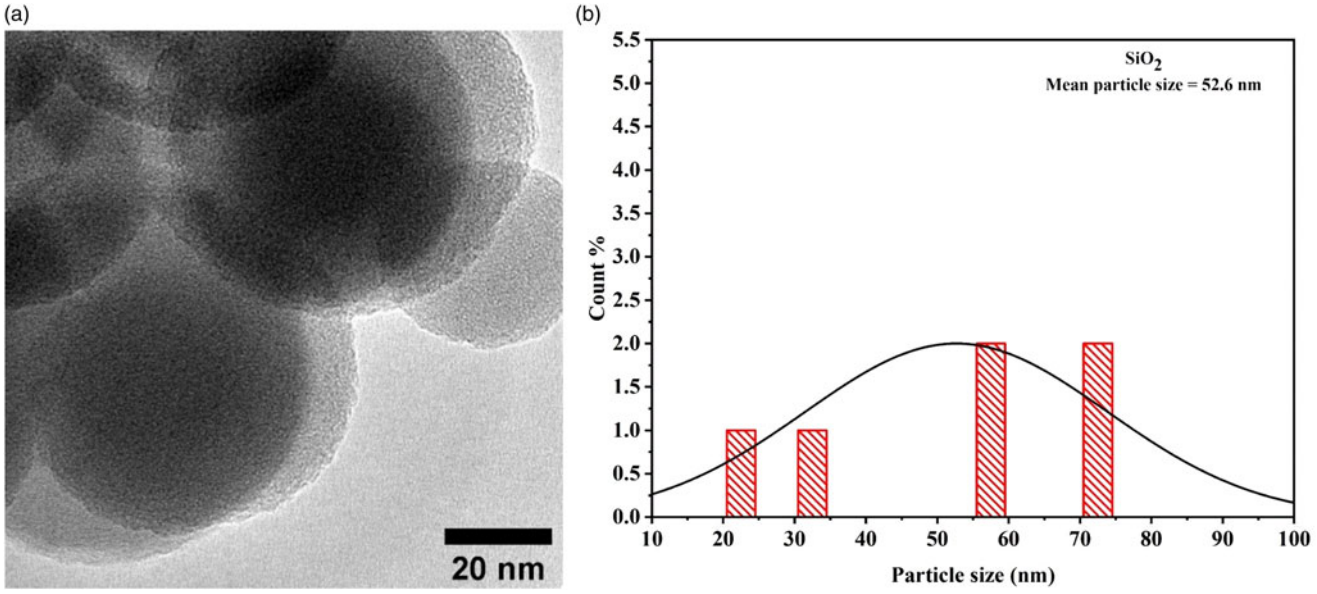

Figure 9. (a) TEM image of silica nanoparticles with potassium hydroxide. (b) Particle-size distribution histogram of silica nanoparticles with potassium hydroxide.

size and agglomerated in morphology with an amorphous nature, as confirmed by SEM, TEM and XRD characterization. The prepared nano-silica with an amorphous nature and a nano size range has potential future scalable applications in the cement industry as a low-cost source material.

Financial support. The authors thank the Higher Education Commission for providing financial support.

Conflicts of interest. The authors declare none.

References

Amin N., Khattak S., Noor S. & Ferroze I. (2016) Synthesis and characterization of silica from bottom ash of sugar industry. *Journal of Cleaner Production*, **117**, 207–211.

Ghorbani F., Younesi H., Mehraban Z., Çelik M.S., Ghoreyshi A.A. & Anbia M. (2013) Preparation and characterization of highly pure silica from sedge as agricultural waste and its utilization in the synthesis of mesoporous silica MCM-41. *Journal of the Taiwan Institute of Chemical Engineers*, **44**, 821–828.

Gu S., Zhou J., Yu C., Luo Z., Wang Q. & Shi Z. (2015) A novel two-staged thermal synthesis method of generating nanosilica from rice husk via pre-pyrolysis combined with calcination. *Industrial Crops and Products*, **65**, 1–6.

Heikal M. (2016) Characteristics, textural properties and fire resistance of cement pastes containing Fe_2O_3 nano-particles. *Journal of Thermal Analysis and Calorimetry*, **126**, 1077–1087.

Heikal M., Ismail M.N. & Ibrahim N.S. (2015) Physico-mechanical, microstructure characteristics and fire resistance of cement pastes containing Al_2O_3 nanoparticles. *Construction and Building Materials*, **91**, 232–242.

Jafarzadeh M., Rahman I. & Sipaut C. (2009) Synthesis of silica nanoparticles by modified sol-gel process: the effect of mixing modes of the reactants and drying techniques. *Journal of Sol-Gel Science and Technology*, **50**, 328–336.

https://doi.org/10.1180/clm.2023.36 Published online by Cambridge University Press

Kanchanason V. & Plank J. (2017) Role of pH on the structure, composition and morphology of C-S-H–PCE nanocomposites and their effect on early strength development of Portland cement. *Cement and Concrete Research*, **102**, 90–98.

Luo K., Li J., Lu Z. Jiang J. & Niu Y. (2019) Effect of nano-SiO_2 on early hydration of natural hydraulic lime. *Construction and Building Material*, **216**, 119–127.

Meng T., Qiang Y., Hu A., Xu C. & Lin L. (2017) Effect of compound nano-$CaCO_3$ addition on strength development and microstructure of cement-stabilized soil in the marine environment. *Construction and Building Material*, **151**, 775–781.

Norsuraya S., Fazlena H. & Norhasyimi R. (2016) Sugarcane bagasse as a renewable source of silica to synthesize Santa Barbara Amorphous-15 (SBA-15). *Procedia Engineering*, **148**, 839–846.

Paya J., Monzo J., Borrachero M.V., Mellado A. & Ordonez L.M. (2001) Determination of amorphous silica in rice husk ash by a rapid analytical method. *Cement and Concrete Research*, 31, 227–231.

She W., Du Y., Miao C., Liu J., Zhao G., Jiang J. & Zhang Y. (2018) Application of organicand nanoparticle-modified foams in foamed concrete: reinforcement and stabilization mechanisms. *Cement and Concrete Research*, **106**, 12–22.

Sikora P., Elrahman M.A., Chung S.Y., Cendrowski K., Mijowska E. & Stephan D. (2019) Mechanical and microstructu]ral properties of cement pastes containing carbon nanotubes and carbon nanotube–silica core–shell structures, exposed to elevated temperature. *Cement and Concrete Research*, **95**, 193–204.

Singh N.B., Kalra M. & Saxena S.K. (2017) Nanoscience of cement and concrete. *Materials Today: Proceedings*, **4**, 5478–5487.

Sun W., Zeng Q. & Yu A. (2013) Calculation of noncontact forces between silica nanospheres. *Langmuir*, **29**, 2175–2184.

Tang Z., Zhang L., Feng W., Guo B., Liu F. & Jia D. (2014) Rational design of graphene surface chemistry for high-performance rubber/graphene composites. *Macromolecules*, **47**, 8663–8673.

Tang Z., Zhang C., Wei Q., Weng P. & Guo B. (2016) Remarkably improving performance of carbon black-filled rubber composites by incorporating MoS_2 nanoplatelets. *Composites Science and Technology*, **132**, 93–100.

Velmurugan P., Shim J., Lee K.J., Cho M., Lim S.S., Seo S.K. *et al.* (2015) Extraction, characterization, and catalytic potential of amorphous silica from corn cobs by sol-gel method. *Journal of Industrial and Engineering Chemistry*, **29**, 298–303.

Wang X.D., Shen Z.X., Sang T., Cheng X.B., Li M.F., Chen L.Y. & Wang Z.S. (2010) Preparation of spherical silica particles by Stöber process with high concentration of tetra-ethyl-orthosilicate. *Journal of Colloid and Interface Science*, **341**, 23–29.

Wassie A.B. & Srivastava V.C. (2017) Synthesis and characterization of nano-silica from teff straw. *Journal of Nano Research*, **46**, 64–72.

Yuvakkumar R., Elango V., Rajendran V. & Kannan N. (2014) High-purity nano-silica powder from rice husk using a simple chemical method. *Journal of Experimental Nanoscience*, **9**, 272–281.

Zhang X., Luo S., Wu X., Feng M., Li Y., Han H. & Li W. (2021) Effect of alkali bases on the synthesis of ZnO quantum dots. *Open Chemistry Journal*, **19**, 377–384.

https://doi.org/10.1180/clm.2023.36 Published online by Cambridge University Press